7th IFAC Symposium on Advances in Automotive Control
The International Federation of Automatic Control
September 4-7, 2013. Tokyo, Japan

Safe Driving Envelopes for Shared Control of Ground Vehicles

Stephen M. Erlien * **Susumu Fujita** ** **J. Christian Gerdes** *

* *Dynamic Design Laboratory, Dept. of Mechanical Engineering Stanford University, Stanford, CA 94305 USA (email correspondence: serlien@stanford.edu)*
** *NISSAN MOTOR Co., Ltd. 1-1 Morinosatoaoyama, Atsugi-shi Kanagawa, 243-0123 Japan*

Abstract: Leveraging new technology in vehicle actuation and sensing, the authors present a control framework for obstacle avoidance and stability control using safe driving envelopes. One of these envelopes is defined by the vehicle handling limits and the other is based on spatial limitations imposed by the environment. A Model Predictive Control (MPC) scheme determines at each time step if the current driver command allows for a safe vehicle trajectory within these two envelopes, intervening only when such a trajectory does not exist. In this way, the controller shares control with the driver in a minimally invasive manner while allowing the driver access to the full capabilities of the vehicle.

Keywords: Vehicle dynamics, vehicle control, stability, envelope, predictive control, obstacle avoidance, shared control

1. INTRODUCTION

A number of new technologies are empowering modern vehicles like never before. Sensing technologies like radar, cameras, and laser systems provide rich information about the environment in real-time. Road surface friction estimates and vehicle states can be made available in real-time in vehicles equipped with steer-by-wire or power-steering as demonstrated by Hsu et al. (2010). In addition, steer-by-wire provides increased actuation capabilities. These new technologies have the potential to make cars much safer.

The predictive nature and constraint handling capabilities of Model Predictive Control (MPC) make it an attractive framework for leveraging these new technologies. Kawabe et al. (2004) present a receding horizon control framework that uses information about the surrounding environment to generate optimal paths to help guide a human driver. Falcone et al. (2007) present a reduced computation MPC scheme for trajectory tracking using active steering actuation.

Recent work has focused on incorporating these techniques into a shared control scheme in which both the controller and a human command the vehicle in a safe manner. Gao et al. (2010) uses a hierarchical MPC controller that separates the obstacle avoidance problem into path planning and path tracking with a given trajectory representing the driver's intent. Anderson et al. (2012) present an MPC controller in a constraint-based, pathless approach to shared control of teleoperated ground vehicles. Their controller's steer command is a weighted blend of the driver's input and the optimal MPC input based on a heuristically determined threat level, and the controller addresses vehicle stability through an objective function which discourages vehicle states away from the origin.

The work in this paper addresses the challenge of shared control with highly capable vehicles through the use of safe driving envelopes, which builds upon successful demonstration of envelope control applied to vehicle stability as presented by Beal and Gerdes (2012). Envelope control is characterized by safe regions of the state space to which the system is constrained and is widely used in aircraft control, as described by Wells (2006). Contributions of this work include an envelope representation of safe driving that incorporates environmental obstacles and vehicle handling limits. The driver's intent is directly incorporated into the MPC objective function resulting in an MPC controller which determines at each time step if the driver's present command allows for a safe trajectory within the safe envelopes, intervening only when such a trajectory does not exist. Variable length time steps in the prediction horizon enables longer look ahead times while still capturing the fast dynamics of the vehicle in the near term. In the initial stage of this work, only front steering actuation is considered with vehicle speed not being controlled and assumed constant. This control scheme is simple enough for fast, real-time implementation and is validated on a vehicle testbed in limited friction environments.

2. VEHICLE MODEL

The vehicle model used in the online MPC controller is a bicycle model with five states: two velocity states and three position states. In this work, only one control input is considered: front steering command (δ).

2.1 Velocity States

The velocity states are sideslip (β) and yaw rate (r) as defined in Fig. 1 and have the following equations of motion:

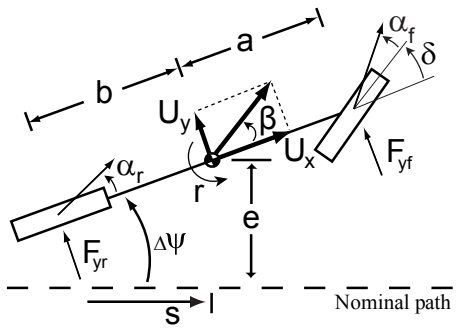

Fig. 1. Bike model schematic

$$\dot{\beta} = \frac{F_{yf} + F_{yr}}{mU_x} - r \qquad \dot{r} = \frac{aF_{yf} - bF_{yr}}{I_{zz}} \tag{1}$$

where $F_{y[f,r]}$ is the lateral tire force of the [front, rear] axle, m is the vehicle mass, U_x is the longitudinal velocity in the body fixed frame, I_{zz} is the yaw inertia, and a and b are the distances from the center of gravity to the front and rear axles, respectively. The tire slip angles, α_f and α_r, can be expressed as:

$$\alpha_f = \tan^{-1}\left(\beta + \frac{ar}{U_x}\right) - \delta \approx \beta + \frac{ar}{U_x} - \delta \tag{2}$$

$$\alpha_r = \tan^{-1}\left(\beta - \frac{br}{U_x}\right) \approx \beta - \frac{br}{U_x} \tag{3}$$

where δ is the front steer angle and small angle approximations give linear expressions. The brush tire model proposed by Fiala (1954) and presented in the following form by Pacejka (2012) gives a useful model of the relationship between $F_{y[f,r]}$ and $\alpha_{[f,r]}$:

$$\begin{aligned} F_y &= -C_\alpha \tan\alpha + \frac{C_\alpha^2}{3\mu F_z}\tan\alpha\,|\tan\alpha| - \frac{C_\alpha^3}{27\left(\mu F_z\right)^2}\tan^3\alpha \\ &= f_{\text{tire}}\left(\alpha\right) \end{aligned} \tag{4}$$

where μ is the surface coefficient of friction, F_z is the normal load, and C_α is the tire cornering stiffness.

The input to the vehicle model is F_{yf}, which is mapped to δ using (2) and (4):

$$\delta = \beta + \frac{ar}{U_x} - f_{\text{tire}}^{-1}\left(F_{yf}\right) \tag{5}$$

where f_{tire}^{-1} is computed numerically and real-time estimates of β and r are assumed to be available. Use of F_{yf} as the model input allows the MPC controller to explicitly consider front tire saturation.

For the rear tires, a linearization of the brush tire model at a given rear tire slip angle, $\bar{\alpha}_r$, models rear tire force, F_{yr}, as an affine function of α_r:

$$F_{yr} = \bar{F}_{yr} - \bar{C}_{\bar{\alpha}_r}(\alpha_r - \bar{\alpha}_r) \tag{6}$$

where $\bar{F}_{yr} = f_{\text{tire}}\left(\bar{\alpha}_r\right)$ and $\bar{C}_{\bar{\alpha}_r}$ is the equivalent cornering stiffness at $\bar{\alpha}_r$. Appropriate choice of $\bar{\alpha}_r$ in the initial time steps of the prediction horizon allows the MPC controller to explicitly consider rear tire saturation in the near term prediction. This will be discussed further in Section 4.

The equations of motion of the velocity states can now be expressed as affine functions of the states and input, F_{yf}:

$$\dot{\beta} = \frac{F_{yf} + \bar{F}_{yr} - \bar{C}_{\bar{\alpha}_r}\left(\beta - \frac{br}{U_x} - \bar{\alpha}_r\right)}{mU_x} - r \tag{7}$$

$$\dot{r} = \frac{aF_{yf} - b\left[\bar{F}_{yr} - \bar{C}_{\bar{\alpha}_r}\left(\beta - \frac{br}{U_x} - \bar{\alpha}_r\right)\right]}{I_{zz}} \tag{8}$$

2.2 Position States

The position states of the vehicle are all in reference to a nominal path that need not be obstacle free. These states are heading deviation ($\Delta\psi$), lateral deviation (e), and distance (s) along the path as defined in Fig. 1.

The equations of motion of the position states can be written as:

$$\dot{\Delta\psi} = r \tag{9}$$

$$\dot{e} = U_x sin(\Delta\psi) + U_y cos(\Delta\psi) \tag{10}$$

$$\dot{s} = U_x cos(\Delta\psi) - U_y sin(\Delta\psi) \tag{11}$$

Using small angle assumptions for $\Delta\psi$ and β, the above nonlinear equations can be approximated as affine functions of the vehicle model states:

$$\dot{e} \approx U_x\Delta\psi + U_x\beta \tag{12}$$

$$\dot{s} \approx U_x - U_x\beta\Delta\psi \approx U_x \tag{13}$$

where, for small values of β and $\Delta\psi$, the product $\beta\Delta\psi \approx 0$.

Combining (7), (8), (9), (12), and (13), a state-space representation of the vehicle model is expressed as:

$$\dot{x} = A_{\bar{\alpha}_r}x + B_{\bar{\alpha}_r}F_{yf} + d_{\bar{\alpha}_r} \tag{14}$$

where $x = [\beta \quad r \quad \Delta\psi \quad s \quad e]^T$ and subscript $_{\bar{\alpha}_r}$ denotes linearization around $\bar{\alpha}_r$.

3. ENVELOPE DEFINITIONS

To ensure safe operation of the vehicle, the controller constrains the states of the vehicle within two safe driving envelopes. The first of these is a stable handling envelope that ensures vehicle stability through constraints on the velocity states. The second is an environmental envelope that constrains the position states to ensure the vehicle trajectory is collision free. The definitions of these envelopes and the methodologies to generate them real-time are presented in the following sections.

3.1 Stable Handling Envelope

Originally presented by Beal and Gerdes (2012), the stable handling envelope is summarized here. The envelope is defined by limits on the vehicle states as illustrated in Fig. 2. This envelope reflects the maximum capabilities of the vehicle's tires; therefore, operation within this envelope ensures the vehicle has the capability to safely remain in the envelope.

A steady-state analysis can be used to determine an appropriate bound on yaw rate that does not exceed the friction capabilities of the vehicle. Considering the steady-state condition of (1), the steady-state yaw rate can be expressed as:

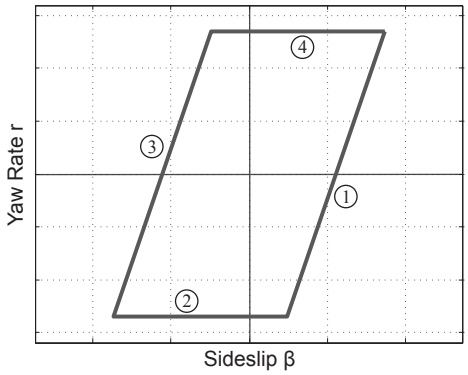

Fig. 2. Stable handling envelope

$$r_{\text{ss}} = \frac{F_{yf} + F_{yr}}{mU_x} \tag{15}$$

Neglecting the effects of weight transfer and assuming zero longitudinal tire forces, the following relationship holds:

$$F_{yf,max} + F_{yr,max} = mg\mu \tag{16}$$

where g is the gravitational constant.

Combining (15) and (16) gives an expression for the maximum steady-state yaw rate which defines bounds (2) and (4) in Fig. 2.

$$r_{\text{ss,max}} = \frac{g\mu}{U_x} \tag{17}$$

Another important consideration for vehicle stability is the saturation of the rear tires. The final two bounds of the vehicle envelope serve to limit the rear slip angle to the angle at which peak lateral force is generated as described by Beal and Gerdes (2012) and expressed as:

$$\alpha_{r,\text{peak}} = tan^{-1}\left(3\frac{mg\mu}{C_{\alpha_r}}\frac{a}{L}\right) \tag{18}$$

Using this expression as a bound on α_r, the following bound on β can be determined from (3):

$$\beta_{\text{max}} = \alpha_{r,\text{peak}} + \frac{br}{U_x} \tag{19}$$

This maximum sideslip serves as the basis for bounds (1) and (3) in Fig. 2. Assuming real-time estimates of μ, r, and U_x are available, the vehicle envelope described is easily calculated real-time and, with appropriately chosen matrices H_{veh} and G_{veh}, can be compactly represented as the linear inequality:

$$|H_{\text{veh}}x| \leq G_{\text{veh}} \tag{20}$$

3.2 Environmental Envelope

Like the position states of the vehicle model, the environmental envelope is in reference to a nominal path and is represented as time-varying constraints on e, the lateral deviation from the nominal path. At each time step, the future trajectory of the vehicle over the prediction horizon is constrained to be within this envelope to ensure the future trajectory of the vehicle is collision free. As mentioned previously, this nominal path need not be obstacle free; therefore, the environmental envelope may require the vehicle to deviate from the nominal path.

Fig. 3 illustrates the methodology to generate the environmental envelope from an arbitrary environment like the one pictured in Fig. 3a. From (13), the vehicle's future position, s, along the path can be determined *a priori* since $\dot{s}$ is a function of only U_x, which is assumed to be known. Therefore, the environment can be sampled at discrete points along the path corresponding to the vehicle's position k steps into the prediction horizon as illustrated in Fig. 3b. In Fig. 3c, the objects in the environment are extended to align with this discrete sampling, and feasible gaps between obstacles are identified producing a conservative representation of the obstacle-free regions of the environment. Feasible gaps are defined as distances greater than the vehicle width.

Simply constraining the vehicle's future lateral deviations to be within these feasible gaps does not ensure a collision free path because the vehicle's trajectory could pass from one side of an obstacle to the other in one time step. Instead, the vehicle's trajectory needs to be fully contained within a *tube* which is defined as a sequence of adjacent feasible gaps along the prediction horizon. Starting at the vehicle's current position and moving in the positive s direction, adjacent feasible gaps are linked together into one of many *tubes* like the one illustrated in Fig. 3d. An important property of these *tubes* is that the set of vehicle trajectories contained within a *tube* is convex and

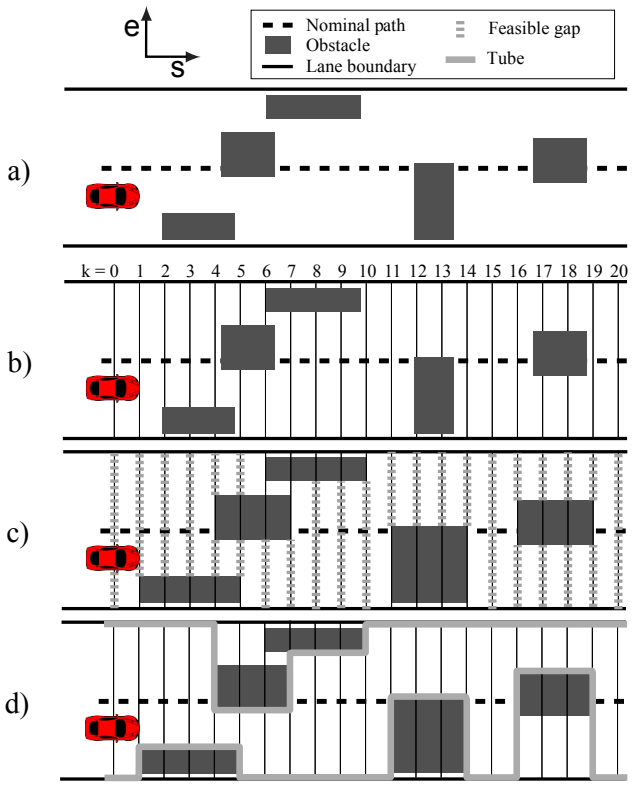

Fig. 3. Generating the environmental envelope from an arbitrary environment

all trajectories in this set are collision free, similar to the homotopies used by Anderson et al. (2012).

Each *tube* provides a bound on e at each time step k and, with appropriately chosen matrices H_{env} and G_{env}, can be compactly written as the linear inequality:

$$H_{\text{env}} x^{(k)} \leq G_{\text{env}}^{(k)} + \frac{1}{2} d_{\text{vehicle}} + d_{\text{buffer}} \tag{21}$$

where d_{vehicle} is the vehicle track width and d_{buffer} specifies a preferred minimum distance between obstacles and the vehicle to ensure driver comfort.

The environmental envelope is defined as the set of *tubes* generated as described above, and a vehicle trajectory is collision free if and only if it satisfies inequality (21) for any *tube* in the environmental envelope. As will be discussed in the next section, the MPC controller will solve a convex optimization problem for each *tube* and the optimal trajectory will be the one corresponding to the tube with the lowest objective value. In this way, dividing the environment into possible *tubes* transforms a challenging, non-convex problem into a set of convex problems which can be quickly solved in parallel.

In the worst-case, this set can be as large as 2^n, with n being the number of obstacles. This occurs in scenarios where each obstacle presents the vehicle with a choice of avoidance on the left or on the right. However, in these scenarios, heuristics could be employed to reduce the number of *tubes* to a representative handful, which could be evaluated in real-time. In addition, the limitation of laser and vision systems to identify objects in these arrangements further supports the use of only a subset of *tubes* to represent the environment. In the current stage of this work, only environments with one obstacle were considered resulting in at most two *tubes*.

4. MPC FORMULATION

The controller's primary task is to ensure safe vehicle operation within the previously defined safe driving envelopes; therefore, these envelopes appear as constraints in the MPC formulation. With these constraints met, it is desirable to be minimally invasive to the driver (i.e., match the driver's present command) while avoiding harsh interventions by the controller (i.e., smooth input trajectories). These last two objectives appear as cost terms in the objective function of the MPC formulation.

4.1 Driver Intent

The desire to match the driver's command is expressed as the cost term:

$$\left| F_{\text{yf,driver}} - \mathbf{F_{yf}}^{(0)} \right| \tag{22}$$

where $F_{\text{yf,driver}}$ is the front tire force corresponding to the driver's steering wheel command (δ_{driver}) and $\mathbf{F_{yf}}^{(0)}$ is the input at the first time step of the MPC optimal trajectory. The brush tire model provides a mapping from δ_{driver} to $F_{\text{yf,driver}}$:

$$F_{\text{yf,driver}} = f_{\text{tire}} \left(\beta + \frac{ar}{U_x} - \delta_{\text{driver}} \right) \tag{23}$$

Cost term (22) uses the l_1 norm for two reasons. First, the desire to *match* the driver's intent is better captured by the larger values of l_1 norm at small deviations than higher order norms. Second, in emergency situations where significant deviations from the driver's intent are required to ensure safety, it is desirable for the controller to ignore the driver altogether. Anderson et al. (2012) achieve this goal through the use of a heuristically determined weighting factor between the driver's command and the MPC optimal command. The l_1 norm provides the best convex approximation to this objective because the value at large deviations is as small as possible while still being convex as discussed by Boyd and Vandenberghe (2004).

4.2 Varying Time Steps

In this work, variable length time steps are employed allowing for a long prediction horizon to account for upcoming obstacles in the long term without compromising the prediction of velocity states in the near term. Therefore, the sampling time (t_s) used to discretize the continuous vehicle model presented in Section 2 is not constant throughout the prediction horizon, but is instead given for the kth step into the prediction horizon by:

$$t_s(k) = \begin{cases} 0.01(s) & 0 \leq k < T_{\text{corr}} \\ t_{\text{corr}} & k = T_{\text{corr}} \\ 0.20(s) & T_{\text{corr}} < k \leq (T-1) \end{cases} \tag{24}$$

where T is the number of steps in the full prediction horizon and t_{corr} is a variable *correction* time step at the T_{corr} step into the horizon whose value ranges from 0.01 to 0.21 (s). The value of t_{corr} is determined on-line by the controller to ensure a consistent representation of the environment during execution. The need for this variable time step is illustrated in Fig. 4. Following the methodology for generating the environmental envelope described in Section 3.2, the boundaries of an obstacle are extended to align with the discretization of the environment. Fig. 4a shows the discretization of the same environment a short time later without an initial correction time step resulting in a different representation of the obstacle; however, if a correction time step of appropriate length is used initially, as in Fig. 4b, the obstacle representation does not change.

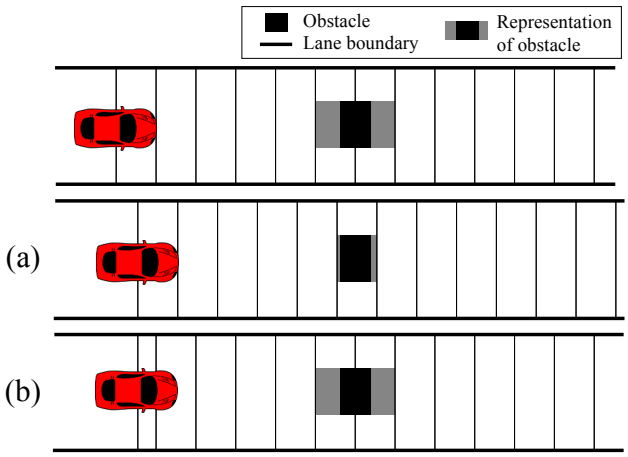

Fig. 4. Representation of the environment re-evaluated a short time later (a) without a correction time step and (b) with a correction time step

4.3 Convex Optimization Problem

The control objectives outlined previously can be expressed as the finite horizon optimal control problem:

$$\underset{\mathbf{F}_{\mathrm{yf}}}{\text{minimize}} \quad \left|F_{\mathrm{yf,driver}} - {\mathbf{F}_{\mathrm{yf}}}^{(0)}\right| \tag{25a}$$

$$+ \gamma \sum_{k=0}^{T-1} \left|\left|{\mathbf{F}_{\mathrm{yf}}}^{(k)} - {\mathbf{F}_{\mathrm{yf}}}^{(k-1)}\right|\right|^2 \tag{25b}$$

$$\text{subject to} \quad x^{(k+1)} = A_{\bar{\alpha}_r} x^{(k)} + B_{\bar{\alpha}_r} {\mathbf{F}_{\mathrm{yf}}}^{(k)} + d_{\bar{\alpha}_r} \tag{25c}$$

$$\left|{\mathbf{F}_{\mathrm{yf}}}^{(k)}\right| \leq F_{\mathrm{yf,max}} \tag{25d}$$

$$\left|H_{\mathrm{veh}} x^{(k+1)}\right| \leq G_{\mathrm{veh}} \tag{25e}$$

$$k = 0 \ldots (T-1)$$

$$\left|{\mathbf{F}_{\mathrm{yf}}}^{(i)} - {\mathbf{F}_{\mathrm{yf}}}^{(i-1)}\right| \leq F_{\mathrm{yf,max\ slew}} \tag{25f}$$

$$i = 0 \ldots T_{\mathrm{corr}}$$

$$H_{\mathrm{env}} x^{(l)} \leq G_{\mathrm{env}}^{(l)} + \tfrac{1}{2} d_{\mathrm{vehicle}} + d_{\mathrm{buffer}} \tag{25g}$$

$$l = (T_{\mathrm{corr}} + 1) \ldots T$$

where $\mathbf{F}_{\mathrm{yf}}$ is the optimal input trajectory and γ is a weighting term establishing the trade-off between a smooth input trajectory (25b) and matching the driver's current steering command (25a).

The vehicle models used in constraint (25c) are discretizations of the continuous vehicle model (14) using the time steps defined by (24) and linearized about $\bar{\alpha}_r$ given by:

$$\bar{\alpha}_r(k) = \begin{cases} \alpha_r^{(0)} & 0 \leq k < T_{\mathrm{corr}} \\ 0 & T_{\mathrm{corr}} \leq k \leq (T-1) \end{cases} \tag{26}$$

where $\alpha_r^{(0)}$ is the current rear slip angle determined by (3) from real-time estimates of β and r. In this way, nonlinear rear tire behavior is accounted for in the first time steps of the prediction horizon.

Constraint (25d) reflects the maximum force capabilities of the front tires and (25f) reflects the slew rate capabilities of the vehicle steering system. It should be noted that the slew rate constraint is *not* enforced during the later portion of the prediction horizon because the large time steps make such a constraint ill-defined. Also, the environmental envelope is not enforced in the early portion of the prediction horizon because the input has little influence on the position states in such a short period of time.

In practice, constraints (25e) and (25g), which correspond to the safe driving envelopes, are softened with slack variables to ensure the optimization is always feasible.

Optimization problem (25) is solved for each *tube* in the environmental envelope and the optimal input corresponding to the *tube* with the lowest objective value is used.

4.4 Implementation

Optimization problem (25) is convex allowing for the use of efficient solvers for real-time implementation. CVXGEN, developed by Mattingley and Boyd (2012), generates a solver that is implemented on a single core of an i7 processor utilizing MATLAB's real-time toolbox. The resulting controller is capable of generating and evaluating two *tubes* in less than 10 [ms] allowing for a controller execution rate of 100 [Hz]. As implemented in the following experiments, $T_{\mathrm{corr}} = 10$ and $T = 30$ giving a look ahead time of 3.91 to 4.11 (s) depending on the present value of t_{corr}.

5. EXPERIMENTAL VALIDATION

Experiments using the test vehicle in Fig. 5 validate the MPC control scheme presented. Testing conditions include a gravel surface with variable friction $\mu = [0.5\ 0.6]$ which was assumed to be a constant $\mu = 0.55$ and vehicle speeds of 8 to 10 $\left(\frac{\mathrm{m}}{\mathrm{s}}\right)$. In future work, the controller could perceive the environment using vision and laser systems; however, for this work, these systems are emulated using prior knowledge of the obstacle and road boundary locations along with an on-board GPS/INS system.

Fig. 5. Stanford's P1 steer-by-wire research testbed

Table 1. P1 Parameters

Parameter	Value	Units
m	1725	kg
I_z	1300	$\mathrm{kg \cdot m^2}$
a	1.35	m
b	1.15	m
$\mathrm{C}_{\alpha f}$	57.8	$\mathrm{kN \cdot rad^{-1}}$
$\mathrm{C}_{\alpha r}$	110	$\mathrm{kN \cdot rad^{-1}}$

Fig. 6 illustrates an experiment simulating a distracted driver. At instance (1) the controller deviates from the driver's command to safely avoid the approaching obstacle while remaining within the road boundaries. The controller matches the driver again at (2) when his command would no longer lead to a violation of the envelope. At (3) the driver approaches the road boundary and the controller makes a minor adjustment to avoid collision.

Fig. 7 illustrates a more challenging test of the controller. At instance (1) the driver executes a *dropped throttle oversteer* maneuver by releasing the accelerator pedal and turning sharply. The combination of weight transfer and regenerative braking significantly reduces the lateral force capabilities of the rear axle inducing limit oversteer behavior. The controller takes appropriate action to stabilize the vehicle and the unmodeled disturbance causes only a slight envelope violation. At (2) the approaching obstacle threatens violation of the environmental envelope and the controller deviates significantly from the driver to safely avoid collision. The controller ignores the extreme commands of the driver until (3).

6. CONCLUSION

Preliminary results demonstrate smooth integration of the controller and driver commands showing promise of this

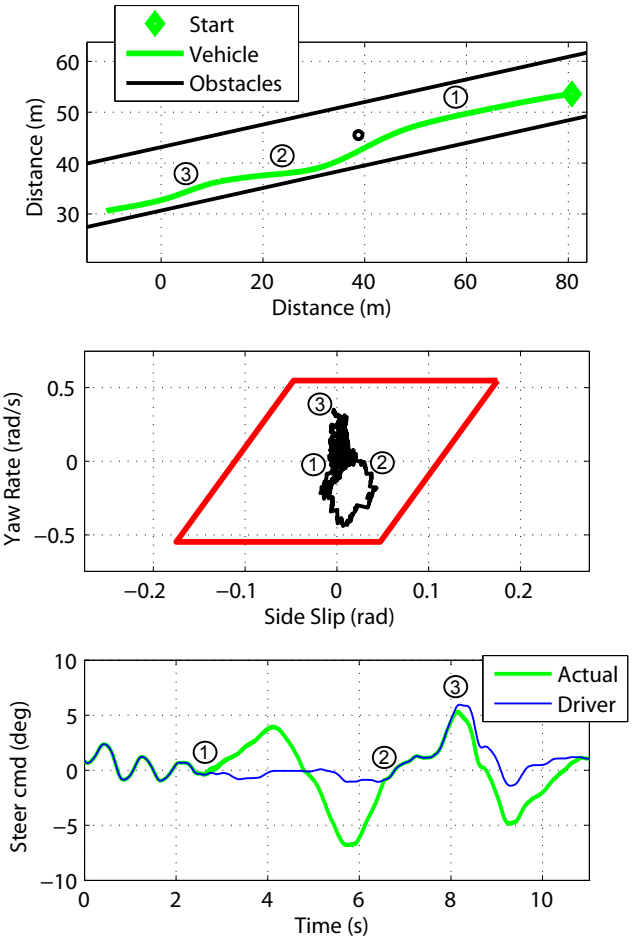

Fig. 6. Experiment simulating a distracted driver

approach as a shared control scheme. In addition, violation of the vehicle stability envelope is minimal even in the presence of unmodeled disturbances and environmental obstacles giving evidence to the stabilizing capability of the controller. Future work focuses on incorporation of moving obstacles and methodologies to leverage brake actuation and variable speed.

ACKNOWLEDGEMENTS

The authors would like to thank the NISSAN MOTOR Co., Ltd. and project team members Yoshitaka Deguchi and Hikaru Nishira for sponsoring this research. The authors also gratefully acknowledge John Kegelman, Daniel Malmquist, and Michael Erlien for their assistance in conducting experiments.

REFERENCES

Anderson, S., Karumanchi, S., and Iagnemma, K. (2012). Constraint-based planning and control for safe, semi-autonomous operation of vehicles. In *Intelligent Vehicles Symposium (IV), 2012 IEEE*, 383–388.

Beal, C.E. and Gerdes, J.C. (2012). Model predictive control for vehicle stabilization at the limits of handling. *IEEE Transactions on Control Systems Technology*.

Boyd, S. and Vandenberghe, L. (2004). *Convex Optimization*. Cambridge University Press, Cambridge, UK.

Falcone, P., Borrelli, F., Tseng, E., J.Asgari, and Hrovat, D. (2007). Linear time-varying model predictive control and its application to active steering systems: Stability analysis and experimental validation. *International Journal of Robust and Nonlinear Control*, 18, 862875.

Fiala, E. (1954). Lateral forces on rolling pneumatic tires. In *Zeitschrit V.D.I*, volume 96.

Gao, Y., Lin, T., Borrelli, F., Tseng, E., and Hrovat, D. (2010). Predictive control of autonomous ground vehicles with obstacle avoidance on slippery roads. In *Dynamic Systems and Control Conference*.

Hsu, Y.H., Laws, S., and Gerdes, J. (2010). Estimation of tire slip angle and friction limits using steering torque. *IEEE Transactions on Control Systems Technology*, 18(4), 896–907.

Kawabe, T., Nishira, H., and Ohtsuka, T. (2004). An optimal path generator using a receing horizon control scheme for intelligent automobiles. In *IEEE International Conference on Control Applications*.

Mattingley, J. and Boyd, S. (2012). Cvxgen: a code generator for embedded convex optimization. *Optimization and Engineering*, 13(1), 1–27.

Pacejka, H.B. (2012). *Tire and Vehicle Dynamics*. Butterworth-Heinemann, 3rd edition.

Wells, K.H. (2006). Aircraft control laws for envelope protection. In *AIAA Guidance, Navigation, and Control Conference*, AIAA-2006-6055.

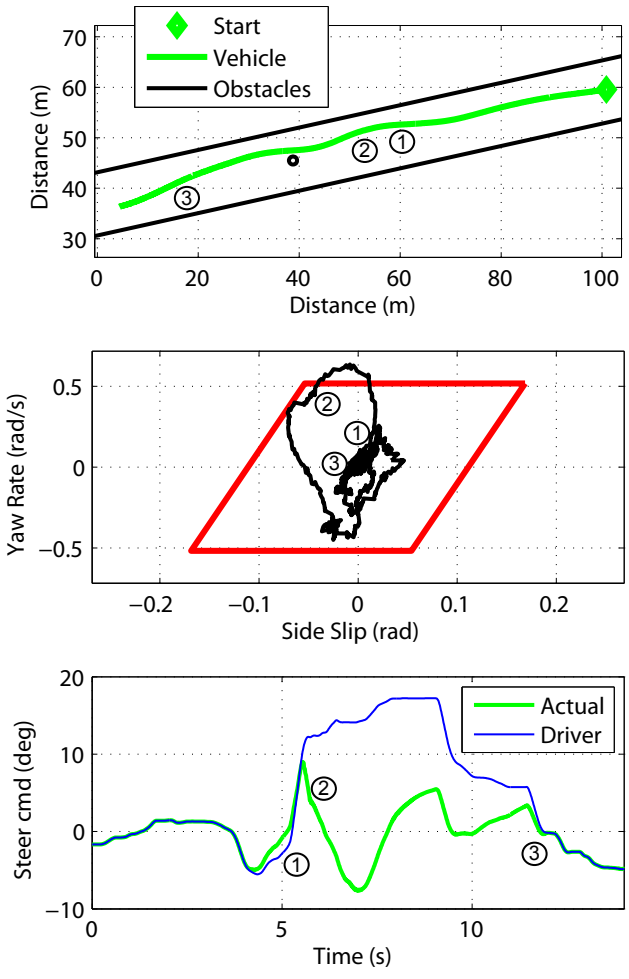

Fig. 7. Experiment with dropped throttle at instance 1